Exotic magnetic anisotropy map in epitaxial $La_{0.7}Ca_{0.3}MnO_3$ films on $BaTiO_3$

A. Alberca,[1] N. M. Nemes,[1,2] F. J. Mompean,[1] N. Biskup,[1] A. de Andres,[1] C. Munuera,[1] J. Tornos,[2] C. Leon,[2] A. Hernando,[3] P. Ferrer,[4] G. R. Castro,[4] J. Santamaria,[2] and M. Garcia-Hernandez[1,*]

[1]*Instituto de Ciencia de Materiales de Madrid, Consejo Superior de Investigaciones Científicas, Sor Juana Inés de la Cruz, 3, ES-28049 Madrid, Spain*

[2]*Departamento de Física Aplicada III, Universidad Complutense, Ciudad Universitaria, ES-28040 Madrid, Spain*

[3]*Departamento de Física de Materiales and Instituto de Magnetismo Aplicado Salvador Velayos, Universidad Complutense, Ciudad Universitaria, ES-28040 Madrid, Spain*

[4]*SpLine Spanish CRG Beamline at the European Synchrotron Radiation Facility, BP 220, FR-38043 Grenoble Cedex 9 (France) and Instituto de Ciencia de Materiales de Madrid, Consejo Superior de Investigaciones Científicas, Sor Juana Inés de la Cruz, 3, ES-28049 Madrid, Spain*

(Received 2 March 2011; revised manuscript received 12 July 2011; published 4 October 2011)

We report the observation between 40 and 120 K of anomalous magnetic hysteresis loops in thin epitaxial films of $La_{0.7}Ca_{0.3}MnO_3$ grown on ferroelectric $BaTiO_3$. These hysteresis loops display extremely unusual features: after switching at coercivity, the magnetization overshoots the eventual high-field value. We study the strains in the film and substrate with x-ray diffraction and propose a model of two magnetic moment populations with different magnetoelastic anisotropies. The relative weights of both populations can be estimated by comparison with twin samples of $La_{0.7}Ca_{0.3}MnO_3$ films on nonferroelectric $SrTiO_3$. We propose that the observed magnetization overshoots the result from differences in the magnetostriction balance as the applied magnetic field increases. The picture of a nonuniform strain field in $La_{0.7}Ca_{0.3}MnO_3$ on $BaTiO_3$, caused by the corrugation of the ferroelectric domains in the rhombohedric phase of $BaTiO_3$, is compatible with the magnetic granular behavior observed in the temperature and field dependences of the magnetization as well as in the low temperature magnetoresistance exhibited by the epitaxial film.

DOI: 10.1103/PhysRevB.84.134402 PACS number(s): 75.25.−j, 75.70.−i, 77.55.Px

I. INTRODUCTION

Recently, multiferroics[1] have become the new paradigm to solve the drawbacks exhibited by only-magnetic (MRAM)[2] or only-ferroelectric-based (FRAM)[3,4] random access memories (RAM). Unfortunately, multiferroics are scarce in nature since ferroelectricity and magnetic ordering require to some extent antagonistic conditions and, consequently, heterostructures combining ferromagnets (FM) and ferroelectrics have emerged as a route to design systems with artificial magnetoelectric coupling and as a feasible alternative to MRAM and FRAM memories. Preliminary results have been obtained by using interfacial coupling of colossal magnetoresistive manganites with piezoelectrics (PZ).[5] The basic idea is that magnetic/charge/orbital ordering in manganites is extremely sensitive to structural changes: distortions away from the ideal cubic perovskite result in a reduction of the band width; epitaxial strain promotes the tetragonal distortion of the octahedra causing Jahn–Teller effects on the Mn^{3+}, which in turn has strong impact on orbital ordering.[6] In heterostructures with stacked PZ/FM epitaxial layers, it seems possible to propagate the strain induced in one component to the other one, either by magnetostriction in the FM or by inverse piezoelectric effect on the PZ. Consequently, the polarization of the PZ may be altered by acting on the magnetic state of the FM or, conversely, the magnetic/charge/orbital state of a magnetoresistive manganite by acting on the PZ by application of an electric field.[7–9] Through its low-temperature structural changes, ferroelectric $BaTiO_3$ (BTO) offers an opportunity to study strain modifications of magnetic and magnetotransport properties. Along this line, epitaxial 500 Å thick $La_{0.7}Sr_{0.3}MnO_3$ films on BTO were studied by Lee *et al.*,[10] demonstrating hysteretic jumps in resistivity and magnetization concomitant to BTO structural phase transitions. Recently, results on the systems $La_{0.7}Sr_{0.3}MnO_3$/PMNT and $La_{0.7}Ba_{0.3}MnO_3$/BTO have been reported.[9,11] Also, various groups have reported that magnetoelastic contributions to anisotropy in magnetite on BTO calculated from experimentally determined strains can account for the observed magnetic anisotropy.[12–14]

Here, we report on the novel magnetic behavior found in thinner epitaxial $La_{0.7}Ca_{0.3}MnO_3$ (LCMO) films on ferroelectric BTO substrates. The choice of materials is determined by the lattice mismatch, the strong tendency of LCMO to phase segregation, and the sensitivity of its equilibrium between phases to strain effects. The two structural phase transitions in ferroelectric BTO take place at $T = 278$ and 183 K. The former, well within the paramagnetic regime, is expected to have little effect on the magnetic or transport properties of LCMO/BTO; however, the latter is near the percolative metal-insulator transition of epitaxial LCMO thin films, and therefore provides an excellent scenario to explore the effect of BTO stress field patterns on the delicate phase segregation map of LCMO. Also, the expected corrugation of the BTO surface within the rhombohedral phase[15] can affect the magnetic domain pattern of the LCMO film, which adds interest to the exploration of the system at temperatures below the BTO rhombohedral phase transition at $T = 183$ K.

As a reference, we chose a twin LCMO film grown on nonferroelectric $SrTiO_3$ (STO). Comparison with a bulk single crystal was ruled out since, when dealing with thin films,

considerations such as oxygen stoichiometry are paramount. Also, both substrates, BTO and STO, are titanates. Thus, a similar chemistry in the sublattice B is expected at the manganite/substrate interface. The reference system, LCMO/STO, complies[16] with what is expected of an epitaxial system providing a good model system for a homogenously strained film, in contrast to the inhomogeneously strained LCMO/BTO.

STO ($a = 3.905$ Å) also provides a template for LCMO epitaxial growth with lattice parameters closer to LCMO bulk ones (pseudocubic $a = 3.86$ Å) than BTO ($a = 3.994$ Å, $c = 4.038$ Å in the tetragonal phase). Strain fields due to lattice mismatch have been proposed and reported to affect the magnetic behavior[17–20] causing changes in the Curie temperature and the saturation magnetic moment, although other variables such as the electronic density map at the interface also play a role. We propose that the new magnetic phenomenology found on LCMO grown on BTO is related to the nonuniformity of the strain fields in the thin film. Beyond the difference in lattice parameters of BTO and STO substrates, the ferroelectric domains present in BTO should be considered the main source of nonuniformity, and so we propose a magnetoelastic anisotropy model for LCMO, incorporating strain values in the proximity to the LCMO-BTO interface different than in the rest of the film.

II. EXPERIMENTAL

Batches of four thin LCMO films (120 Å) were prepared simultaneously on unpoled (001) BTO and (001) STO ($5 \times 5 \times 1$ mm^3) single-crystal substrates by sputtering (5 Å/min deposition rate) in a highly oxidizing plasma (3.4 mbar oxygen atmosphere) at high temperatures (1173 K), well above the BTO ferroelectric Curie point (393 K). Sample batches were annealed in 700 mbar O_2 (1 h at 993 K) and cooled at 5 K/min. Sample thicknesses were determined by x-ray reflectometry. Grazing incidence (GIXD) and coplanar (XRD) synchrotron x-ray diffraction measurements of as-prepared samples were conducted during two campaigns at the ESRF SpLine beamline (BM25B).[21] Initially, data were taken as a function of temperature in the tetragonal (T), orthorhombic (O), and rhombohedra (R) phases of BTO down to 132 K. The second campaign was devoted to further explore the R phase with measurements in the 93–180 K range in a magnetically equivalent sample of the same LCMO thickness. All synchrotron measurements were done with incident energy of 15 keV resulting in extinction lengths close to 0.4 μm for GIXD and 1.2 μm for XRD.

Before magnetization measurements, the LCMO/BTO sample was poled by applying a 200-V dc voltage between the LCMO and a bottom silver electrode and then discharged. Polarization hysteresis loops show that 200 V is sufficient to fully pole the BTO substrate. Room temperature four-circle XRD measurements with Cu $K_{\alpha 1}$ radiation (extinction length 6.8 μm, beam size 3×5 mm^2) and a position sensitive detector on LCMO/BTO samples as a function of applied electric field showed polarization of BTO (absence of *a* ferroelectric domains[15]) above 120 V/mm and the presence of both *a* and *c* domains at ferroelectric remanence. Magnetization, *M*, was measured in a vibrating sample magnetometer (VSM), following zero field cooled (ZFC) and field cooled (FC) protocols. The temperature dependence of the magnetization was measured in 100 Oe applying the magnetic field along the LCMO film plane and coinciding with the (100) axis of the BTO or STO substrate. Hysteresis cycles were measured in the parallel configuration and for LCMO/BTO also with the applied field perpendicular to the film. Additionally, low-temperature magnetoresistance was measured with magnetic field applied in plane along (100), with contacts in the van der Pauw configuration. The surface morphology of both LCMO/BTO and LCMO/STO samples was investigated with scanning force microscopy (AFM) in ambient conditions using a commercial AFM from Nanotec. Images were acquired in contact mode with commercial silicon tips (Nanosensors PPP-FMR).

III. RESULTS

Figures 1(a)–1(c) show coplanar XRD maps near BTO pseudocubic (001) + (100) reciprocal space points in the T, O, and R phases. Crucially, the LCMO film remains epitaxial at all temperatures. In grazing incidence x-ray diffraction (GIXD) near the (1 −1 2) reflection, lattice parameters were determined from BTO and (thickness broadened) LCMO peaks. At all temperatures, with the exception of 250 K, lattice parameters *a* and *b* of LCMO remain larger than the pseudocubic bulk value ($a_P = 3.86$ Å), while *c* remains smaller. We do not have an explanation for the anomalous observation at $T = 250$ K. Strains $\varepsilon_{\alpha\alpha} = (\alpha - a_P)/a_P$ with $\alpha = a, b, c \equiv x, y, z$ were calculated for both BTO and LCMO and are shown in Fig. 1(d). Note, that high-resolution neutron powder diffraction of BTO reveals that there is hardly

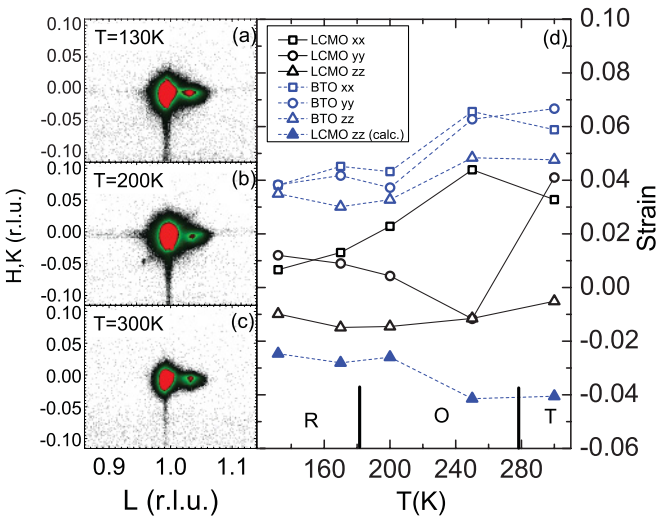

FIG. 1. (Color online) Coplanar XRD reciprocal space maps of LCMO/BTO in the BTO T, O and R phases [(a) 130, (b) 200, and (c) 300 K, respectively]. The broad central features near $L = 1.00$ correspond to intense, saturated, BTO reflections. The LCMO reflections appear close to $L = 1.03$. (d) Temperature dependence of strains relative to LCMO pseudocubic bulk parameter for BTO and LCMO (open symbols), LCMO ε_{zz} in biaxial approximation from BTO strain values: $\varepsilon_{zz} = -(c_{12}/c_{11})(\varepsilon_{xx} + \varepsilon_{yy})$, suitable to describe the strain field in the LCMO layers closer to BTO (full symbols). Vertical bars indicate BTO structural phase transitions.

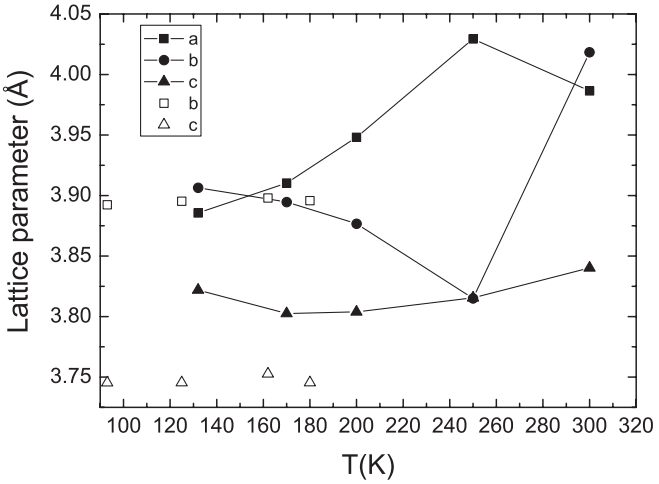

FIG. 2. Lattice parameters for LCMO determined from GIXD. Closed and open symbols refer to two different samples. Closed symbols were obtained from measurements near BTO (1 −1 2), and open symbols were obtained from measurements near BTO (0 −1 1). Lines are guides to the eye.

any change in its lattice parameters below $T = 130$ K (the maximum change in the fitted lattice parameter throughout the R phase corresponds to 5×10^{-4} at 150 K, relative to the experimental value at 15 K)[22] and no transition occurs in bulk LCMO, either. On this basis, no additional strain sources are expected, other than thermal contraction of the lattices. Since our experimental data contain two points in the rhombohedral phase of BTO, we adopt the resulting strain fields in our analysis throughout the R phase. The limits of validity of this assumption were experimentally verified by the second campaign of GIXD measurements near (0 −1 1) on a different, but magnetically equivalent, LCMO/BTO sample at three additional temperatures in the R phase. Figure 2 shows the temperature dependence of the lattice parameters of LCMO for both samples. In spite of the disparity in the absolute value of the out-of-plane lattice constant of the samples in the R phase, the maximum measured changes of the in-plane and out-of-plane LCMO lattice constants within the 93–180 K temperature range amount, respectively, to 1×10^{-3} and 2×10^{-3} of the value at 93 K for the second sample and do not alter our subsequent line of reasoning. Structural coherence lengths estimated from the widths of the GIXD (1 −1 2) diffraction peaks are approximately constant in temperature and range from 200–250 Å in plane and 70–100 Å out of plane (smaller than the measured film thickness of 120 Å) for LCMO. This leaves a 5-nm difference along the out-of-plane direction in LCMO and supports the choice of a model with two regions along the normal to the BTO-LCMO interface in which each region is characterized by a different strain field, as described below. An experimental diffraction study of in-plane strain variations was not possible due to the large footprint of the incident beam in GIXD geometry. Microdiffraction measurements in the room temperature (T) phase of BTO have reported strains $\Delta c/c$ in the range of 10^{-5} along the BTO surface normal with variations in the micron scale due to the alternation of a and c domains.[23]

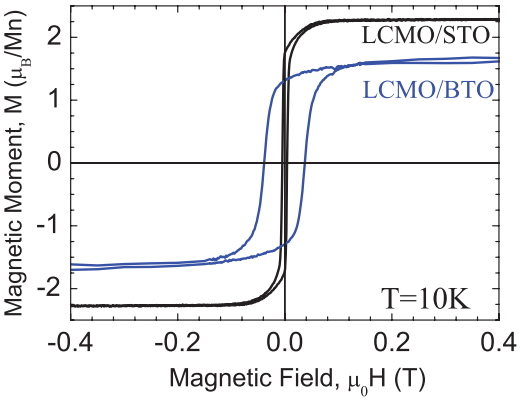

FIG. 3. (Color online) Hysteresis cycles for LCMO/BTO (blue) and LCMO/STO (black) at 10 K.

Magnetization hysteresis loops (Fig. 3) and temperature dependence (Fig. 4) of LCMO/BTO are compared to those of LCMO/STO. The Curie temperature, T_C, is depressed from the 270 K bulk value to about 200 K on BTO and slightly above 150 K for LCMO on STO.[16] The low-temperature saturation magnetic moment is also reduced from the limiting 3.7 μ_B/Mn to 2.3 μ_B/Mn in LCMO/STO and to 1.6 μ_B/Mn on LCMO/BTO. Large differences are apparent between the two samples in the temperature dependence of the ZFC magnetization and in the temperature dependence of the

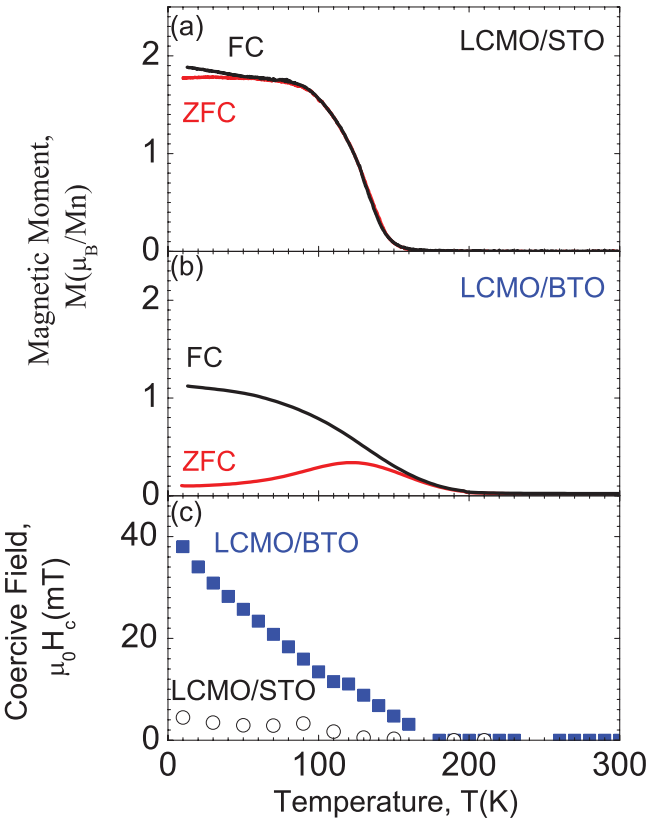

FIG. 4. (Color online) Magnetization vs temperature of (a) LCMO/STO and (b) LCMO/BTO for zero-field (red) and field cooled (black) runs. (c) Coercive field for LCMO/BTO (blue squares) and LCMO/STO (black circles)

coercive fields. For LCMO/BTO, the temperature dependence of M exhibits strongly diverging zero field cooled (ZFC) and field cooled (FC) curves with a broad maximum centered at 120 K [Fig. 4(b)]. Irreversibility hardly occurs for the LCMO/STO system. The coercive field, H_c [Fig. 4(c)], of LCMO/BTO rises linearly with decreasing T, while saturation at low T is observed for LCMO/STO. Here, H_c for LCMO/BTO is very large, above 500 Oe, at low temperature; whereas for LCMO/STO, it is around 40 Oe. This signals either a much larger number of defects or the presence of additional anisotropy sources in LCMO/BTO as compared to LCMO/STO. The large irreversibility observed in LCMO/BTO, the feature around 120 K similar to a blocking temperature, and the linear temperature dependence of H_c point towards a kind of magnetic granular system,[24] rather than to a canonical, collinear ferromagnet. Note that we do not refer to a granular structure in the sense of a polycrystalline film but to a system exhibiting an inhomogeneous magnetic behavior, although the limited structural coherence resulting from the inhomogeneous strain map could be interpreted as a structural correlate for the magnetic granular system.

A remarkably anomalous behavior of the hysteresis cycles of LCMO/BTO was found for 40 K $< T <$ 120 K. Since no phase transition occurs for BTO in this temperature range, the observed behavior could be related to the corrugation expected to develop in the rhombohedral phase.[15] An example is shown in Fig. 5 at 100 K, near the ZFC maximum, where the effect is most pronounced. After switching at H_c, the magnetization overshoots the high field value, M_s, i.e. a fraction of the spins cannot remain aligned with the applied field as it steadily increases. This excess magnetization, ΔM in Fig. 5, is symmetric in both branches of the cycle and at 100 K corresponds to almost 21% of the maximum moment reached. Here, ΔM and the difference between the high field moment in LCMO/BTO and in LCMO/STO normalized to the saturation value in

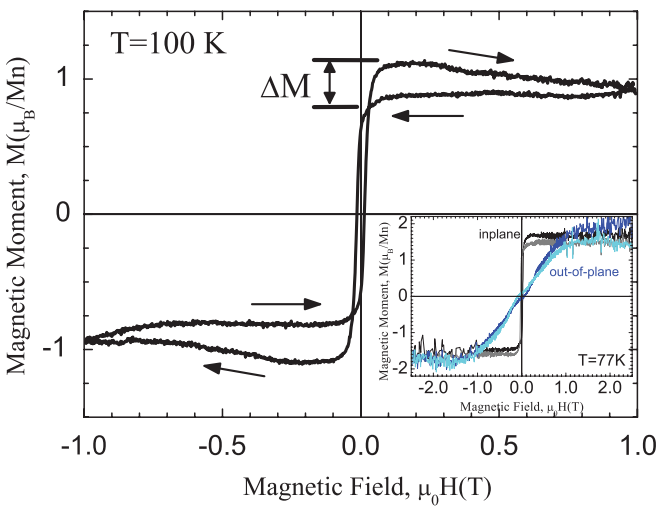

FIG. 5. (Color online) Exotic, Matteucci-like cycle at 100 K of LCMO/BTO showing excess magnetization, ΔM. Inset: Hysteresis cycles with magnetic field in plane (black) and out of plane (blue) of LCMO/BTO at 77K. Increasing field in black and dark blue; decreasing field in gray and light blue: note the Matteucci effect at low field in both orientations.

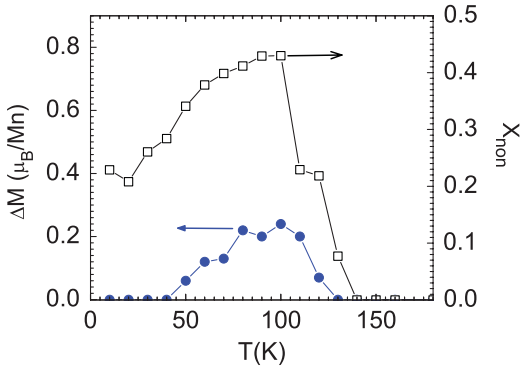

FIG. 6. (Color online) Temperature dependence of ΔM, the excess magnetization observed in Matteucci-like hysteresis cycles (full circles) and x_{non}, the fraction of nonaligned magnetic moments, estimated as $[1 - M_s\ (\text{LCMO/BTO})/M_s(\text{LCMO/STO})]$ (open squares).

LCMO/STO and show the same temperature dependence in the 50–120 K range, as shown on Fig. 6. The excess magnetization ΔM relaxes, decaying linearly with a time constant of $10^{-3}\mu_B$/Mn/min as determined by Superconducting Quantum Interference Device (SQUID) magnetometry at 100 K and −0.5 T, following sample saturation at 5 T. Similar hysteresis loops (termed Matteucci or inverse Wiedemann cycles) have been observed in metal bars under torsion stress fields that induce helical arrangements of magnetization.[25] These Matteucci cycles are not mere minor loops. The inset of Fig. 5 shows magnetization hysteresis loops up to 2.5 T field, applied both in plane, along (100), and out of plane, along (001) on a similar LCMO/BTO sample. The Matteucci effect persists in both orientations in low field, even though magnetic fields as large as 5 T were applied. Also, the out-of-plane cycle slightly crosses the in-plane cycle above 1 T, hinting at some missing moment in the parallel orientation. Note that the noisy trace of the cycles in the inset of Fig. 5 cannot be attributed to instrumental noise but rather to a nonequilibrium condition of the magnetic moments in the sample, as also indicated by the relaxation of ΔM.

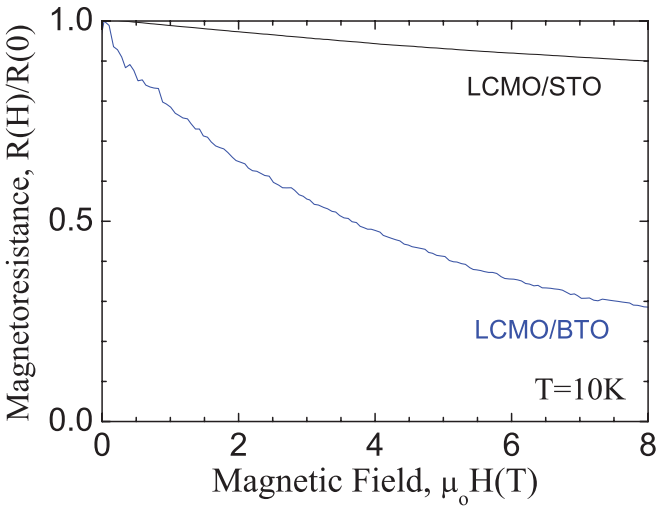

FIG. 7. (Color online) Magnetoresistance at $T = 10$ K for LCMO/STO (black) and LCMO/BTO (blue).

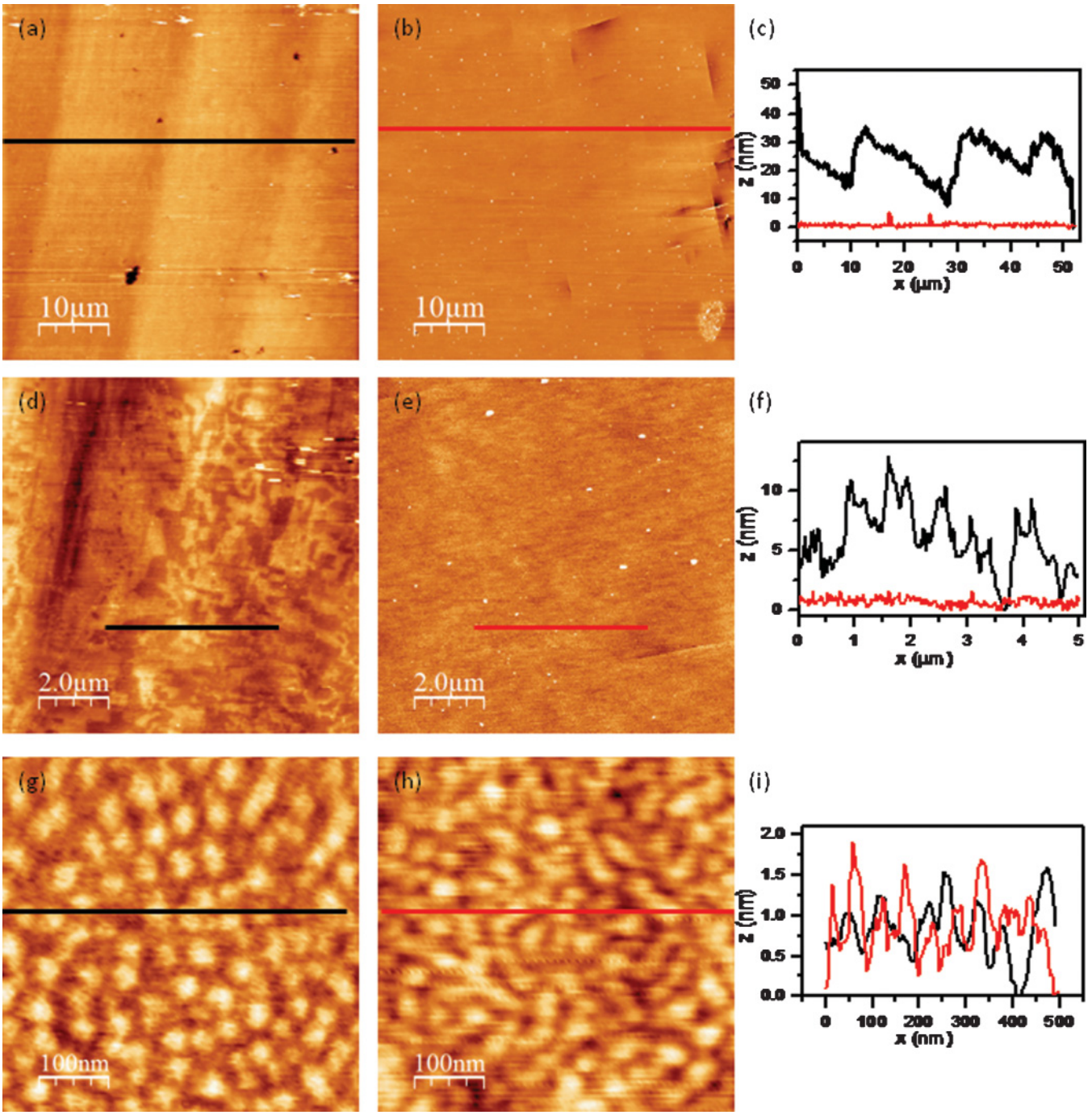

FIG. 8. (Color online) Room temperature AFM topographic images of (a), (d), and (g) LCMO/BTO and (b), (e), and (h) LCMO/STO samples on different length scales and profiles taken along the lines marked on the corresponding images (c), (f), and (i).

Figure 7 shows the field dependence of the magnetoresistance (MR) at low temperature. Note that the behavior observed for LCMO/STO complies with that expected for a uniformly strained epitaxial film: low resistivity ($\sim\rho_0 =$ 200 $\mu\Omega$-cm in $H = 0$) and small MR (approx. 1%/T) whereas LCMO/BTO shows larger MR ratios at low temperature (approx. 10%/T) as well as three orders of magnitude larger resistivity ($\sim\rho_0 = 200$ mΩ-cm in $H = 0$). However, the field dependence of the MR in LCMO/BTO, tending to decrease steadily with field, does not correspond to that expected for a polycrystalline thin film, with a sharp decrease of MR at low fields and small variation at high field. This situation very much resembles that reported for double perovskites with some disorder in the B sublattice, where it was explained in terms of the presence of highly frustrated spin regions located at the interfaces between patches dominated by ferrimagnetic or antiferromagnetic correlations.[26]

Figure 8 shows the AFM topographic images and selected profiles of both samples at room temperature. A noticeable difference is again observed when comparing the surface

morphology. On large length scales, the LCMO/BTO surface shows a corrugation in the micron range that yields a mean roughness of 12 nm [Fig. 8(a)], whereas the LCMO/STO sample shows a flat surface with a mean roughness of 1 nm [Fig. 8(b)]. This difference is better observed in the profiles of Fig. 8(c), and can be ascribed to the different morphology of the corresponding substrates. Figures 8(d) and 8(e), corresponding to the microscale morphology, still show considerable differences, yielding rms values of 4 nm vs 0.6 nm for the LCMO/BTO and LCMO/STO, respectively. Nevertheless, on the nanometer scale [Figs. 8(g) and 8(h)], both crystalline substrates provide flat support for the epitaxial LCMO, with similar surface roughness of 0.5 nm, for both samples. The small grains observed in both samples are probably due to carbonation of the LCMO surface over time in ambient conditions.

IV. DISCUSSION

The picture that emerges for LCMO/BTO is that of an epitaxial film with a finite in-plane and out-of-plane structural coherence. However, the observed magnetic response is akin to a granular system (i.e. the coercive field of the BTO/LCMO rises linearly with decreasing temperature up to a large value of approximately 500 Oe, typical of strongly hindered, interlinked granular systems). Therefore, we refer to it as a magnetically granular system. A most outstanding feature is found: the anomalous hysteresis cycles in the 40–120 K temperature range. These can only be understood in terms of a fraction of spins that move out of plane when the applied field increases. The large coercive field points to a very distinctive anisotropy map when compared to LCMO/STO. Low temperature transport data confirm the image of a magnetically inhomogeneous system. From the AFM topography a noticeable roughness is apparent, due to the inhomogeneous ferroelectric domain map of BTO.

In order to rationalize, on qualitative grounds, the anomalous behavior of the magnetic cycles of LCMO/BTO and prompted by their similarity to Matteucci cycles, we propose a magnetoelastic interpretation. We follow the ideas of the model developed by Vaz *et al.*[13] and Sterbinsky *et al.*[14] for the case of magnetite on BTO. The model assumes that there exists some magnetic moment misalignment induced by the presence of significant stress fields that arise due to the inhomogeneous ferroelectric domain map of the substrate. To account for magnetoelastic anisotropy effects, the model introduces two effective magnetization populations within the LCMO thin film: aligned and nonaligned with the in-plane applied magnetic field, with relative abundance fractions x_{align} and x_{non}, respectively. Relying on the comparison with the more uniformly stressed LCMO/STO sample we estimate $x_{\text{non}} = [1 - M_s\ (\text{LCMO/BTO})/M_s(\text{LCMO/STO})]$ from the corresponding high field magnetizations at each temperature (see Fig. 6). Note that a magnetic dead layer may be present in LCMO/STO films.[27] Previous studies of our LCMO/STO films do not exhibit any change in the saturation magnetization down to approximately 2 nm.[16] Therefore, we only consider the effect of an eventual dead layer that is at most 2 nm thick. This would increase the apparent M_s(LCMO/STO) value rendering higher values for x_{non}. We assume for our thin film a pseudomorphic cubic LCMO structure undergoing elastic deformations leading to tetragonal symmetry. The magnetoelastic anisotropy free energy (F) is given by the sum of the contributions from both magnetic moment populations:

$$F = F_{\text{M,align}} x_{\text{align}} + F_{\text{M,non}} x_{\text{non}} \tag{1}$$

where

$$F_{\text{M}} = [(K_t \cos 2\phi + K_o \sin 2\phi) \sin^2\theta + K_p \cos^2\theta] \tag{2}$$

where θ is the angle between $\boldsymbol{M}$, the magnetization vector, and the surface normal, ϕ is the angle between the projection of $\boldsymbol{M}$ on the sample surface and the applied magnetic field, $\boldsymbol{H}$, and the coefficients K_t, K_o and K_p represent, respectively, contributions arising from tangential and orthogonal (both in plane) and perpendicular (out of plane) $\boldsymbol{M}$ components with respect to $\boldsymbol{H}$. The K coefficients can be calculated from the strain tensor components determined from diffraction experiments, using literature values for the elastic constants c_{11}, c_{12}, and c_{44} and the saturation magnetostriction constants λ_{100} and λ_{111}: $K_t = B_1\ (\varepsilon_{xx} - \varepsilon_{yy})/2$, $K_o = B_2\varepsilon_{xy}/2$ and $K_p = B_1[1 + c_{11}/(2c_{12})]\varepsilon_{zz}$ with $B_1 = 3\lambda_{100}\ (c_{12} - c_{11})/2$ and $B_2 = -3\lambda_{111}c_{44}$.[28,29] For a thin film, shape anisotropy would favor $\theta = 90^\circ$ and an optimal value for ϕ determined by the ratio K_t/K_o. However, it should be kept in mind that our LCMO/BTO sample exhibits characteristics proper of a kind of inhomogeneous magnetic granular system, and therefore the restriction imposed by the shape anisotropy may be relaxed. Also, because of the small weight estimated for the shear strain ($\varepsilon_{xy} \approx 3.5 \times 10^{-3}$), K_o is small and F is almost insensitive to the in-plane angle, ϕ. Thus, we set $\phi = 0$ and are left with the K_t and K_p terms to analyze the contributions of aligned and nonaligned populations to system stabilization.

From our in-plane and out-of-plane measurements, it is clear that the nonaligned population contributes, at least partially, to an out-of-plane magnetization component, compatible with a magnetic granular picture minimizing the shape anisotropy contribution. This picture is further supported by the limited coherence of the structural domains (200 Å in plane and 70 Å out of plane, smaller than sample thickness), as measured by diffraction techniques in LCMO/BTO. Furthermore, we assume that nonaligned spins lay close to the interface with BTO, although some contribution from in-plane segregation might also be conceivable. This is a plausible assumption given the limited out-of-plane structural coherence of our film (70 Å), although, in the rhombohedral phase, we do not discern two resolved components in the diffraction pattern of LCMO but only a broad single feature. We then characterize the LCMO/BTO interface with a biaxial in-plane strain state with values for ε_{xx} and ε_{yy} taken directly from BTO GIXD measurements and ε_{zz} derived from the biaxial strain field as $\varepsilon_{zz} = -(c_{12}/c_{11})(\varepsilon_{xx} + \varepsilon_{yy})$, a reasonable assumption for epitaxial growth. The aligned population is characterized by $\theta = 90^\circ$ and its strain field determined from LCMO GIXD measurements. The resulting nonuniform strain field in our thin LCMO film indicates higher relaxation away from the LCMO-BTO interface [compare full triangles and open triangles in Fig. 1(d)]. Evaluating (1) with the above-mentioned assumptions and the literature value for $\lambda_{100} = +7 \times 10^{-5}$ for both aligned and nonaligned populations, we obtain only

a marginal stabilizing effect from the aligned population contribution to F, irrespective of the fraction of nonaligned moments: with our strain fields and positive magnetostriction, an out-of-plane nonaligned population does not contribute to system stabilization (since $B_1 > 0$). Within the limitations of our model, such stabilization can only be introduced by a change of sign in B_1 for the nonaligned population. This sign reversal may result from a negative value of the saturation magnetostriction λ or, away from cubic symmetry, from a change in the orientation of the LCMO cells (a, b, c) closer to the BTO interface with respect to the (x, y, z) laboratory axes or by a combination of both effects. Since our experimental input comes from macroscopic magnetic and averaged structural magnitudes, we cannot identify on microscopic grounds the mechanism operating in LCMO/BTO. However, if our model is evaluated with $B_1 < 0$ for the nonaligned population, for example by taking λ_{100} (nonaligned) $= -\lambda_{100}$ (aligned), the perpendicular (K_p) stabilizing effect of a very small fraction of nonaligned moments (1%) results in $F < 0$ with wide minima around $\theta = 0^\circ$, which becomes deeper with increasing x_{non}. Thus, fractions of nonaligned moments close to $x_{\text{non}} = 0.43$, the value registered at 100 K at the peak of the anomalous effects, would contribute to the system stabilization. Negative values of the magnetostriction through Villari reversal are not uncommon in systems showing Matteucci and inverse Wiedemann effects like metallic glasses under torsion stress along the applied field axis.[30,31] In manganites, a sign reversal in the magnetic anisotropy with (110) easy axis was reported by Ziese *et al.*[32]

By analogy with the Matteucci systems and bearing in mind the stabilizing effect of the K_p term for such a population of nonaligned moments at saturation (high fields), we propose that noncollinear arrangements of magnetic moments occur in our thin LCMO/BTO films that are responsible for the anomalous cycles. Furthermore, since corrugation imposed by ferroelectric domains is expected in the rhombohedral phase of BTO,[15] noncollinear (for instance helical, in view of the Matteucci-like magnetic hysteresis phenomenology) arrangements can be expected to be located at the peaks and valleys generated at the BTO interface by the corrugation where two different ferroelectric domains meet. These would be highly frustrated regions responsible for the time-dependent behavior observed in the magnetic response. Room temperature AFM images reveal, as expected, different length-scale dependent morphology for the STO and BTO substrates. Note that the particular distribution of FE domains is unique for each sample and varies with its thermal history. We have observed the same effect reported here in a variety of samples (as prepared, poled, and annealed), with small sample-dependent details but with the same basic phenomenology. The existence of regions dominated by K_t and K_p would explain the limited structural coherence of the epitaxy and the observed magnetic granular behavior of LCMO/BTO. Excess magnetization, ΔM, as shown by LCMO/BTO in the temperature range 40 K $< T <$ 120 K would result from the in-plane alignment of a majority of magnetic moments immediately after the application of the coercive field. As the applied field increases, the growth of the aligned domains is hindered by the strong pinning to BTO ferroelectric domains, triggering the switch to out-of-plane orientations of a substantial fraction of the moments and thus increasing the number of moments involved in magnetic domain walls exhibiting helical arrangements. The high-field balance of this competition of magnetostriction effects would be established, as described by our model, with a substantial fraction of the moments lying out of plane, stabilizing the system, and giving rise to a depressed in-plane magnetization.

We address the question of whether the observed phenomenology matches what is expected for the phase-segregation (PS) scenario, given the strong tendency of LCMO to it. PS in the interface of LCMO grown on different substrates is apparent around T_C (T_{MI}) and evolves steadily to a predominantly single phase system as the temperature is lowered. However, the anomalous behavior in the LCMO/BTO magnetization cycles is maximum around 100 K, well below T_C and far apart from the region where conventional PS is maximal. Therefore, conventional phase segregation as that observed in many LCMO systems (see for instance Ref. 33 on phase segregation of LCMO on STO and NGO) cannot be at the root of the observed behavior in LCMO/BTO. Certainly, the observed magnetic behavior results from an inhomogeneous structural scenario within the epitaxial film, and since inhomogeneous strains can result in different magnetic interactions; our magnetically granular system could be considered as a kind of phase-segregated system only in a very broad sense. This is in contrast to what is observed in LCMO/STO, a system for which a canonical PS scenario is ascribed.[6,33]

V. CONCLUSIONS

In conclusion, thin epitaxial films of LCMO/BTO systematically exhibit anomalous Matteucci-like hysteresis cycles around 120 K, the crossover temperature in ZFC magnetization. As in granular systems, this temperature signals the set in of a dominant anisotropy: nonuniform strains in LCMO generate a significant out-of-plane magnetic anisotropy. The observed phenomenology cannot be explained in terms of conventional PS. Helical arrangements of the spins, similar to those exhibited by Matteucci systems may be responsible for the anomalous cycles. Their precise locations as well as their origin remain open questions, since no structural anomaly has been reported for BTO below 180 K. However, corrugation is expected in the rhombohedral phase of BTO and a low temperature AFM study seems in order. Also, whether these helical arrangements could mimic the magnetic structure of natural multiferroics, or are indications of artificial multiferroics, remains to be explored on microscopic grounds. The miniaturization of manganite/PZ heterostructures, by reducing the thickness of the PZ and the manganite surface area, may lead to the controlled manipulation of the spins in those regions and define new concept devices with applications in spintronics.

ACKNOWLEDGMENTS

We acknowledge financial support from MICINN grants MAT2008-06517-C02-01, CSD2009-00013, MAT2008-06517-C02-02, and PI2010-60E013 and provision of beamtime by the European Synchrotron Radiation Facility.

*Corresponding author: marmar@icmm.csic.es

[1]M. Gajek, M. Bibes, S. Fusil, K. Bouzehouane, J. Fontcuberta, A. Barthelemy, and A. Fert, Nat. Mater. **6**, 296 (2007).
[2]C. Chappert, A. Fert, and F. Nguyen van Dau, Nat. Mater. **6**, 813 (2007).
[3]J. S. Moodera, L. R. Kinder, T. M. Wong, and R. Meservey, Phys. Rev. Lett. **74**, 3273 (1995).
[4]J. M. Daughton, J. Appl. Phys. **81**, 3758 (1997).
[5]S. Mathews, R. Ramesh, T. Venkatesan, and J. Benedetto, Science **276**, 238 (1997).
[6]E. Dagotto, *Nanoscale Phase Separation and Colossal Magnetoresistance: The Physics of Manganites and Related Compounds*, (Springer, Berlin, 2002).
[7]C. Thiele, K. Dörr, S. Fähler, L. Schultz, D. C. Meyer, A. A. Levin, and P. Paufler, Appl. Phys. Lett. **87**, 262502 (2005).
[8]W. Eerestein, N. D. Mathur, and J. F. Scott, Nature (London) **442**, 759 (2006); W. Eerenstein, M. Wiora, J. L. Prieto, J. F. Scott, and N. D. Mathur, Nature Mater. **6**, 348 (2007).
[9]C. Thiele, K. Dörr, O. Bilani, J. Rödel, and L. Schultz, Phys. Rev. B **75**, 054408 (2007).
[10]M. K. Lee, T. K. Nath, C. B. Eom, M. C. Smoak, and F. Tsui, Appl. Phys. Lett. **77**, 3547 (2000).
[11]R. K. Zheng, Y. Jiang, Y. Wang, H. L. W. Chan, C. L. Choy, and H. S. Luo, Phys. Rev. B **79**, 174420 (2009)
[12]H. F. Tian, T. L. Qu, L. B. Luo, J. J. Yang, S. M. Guo, H. Y. Zhang, Y. G. Zhao, and J. Q. Li, Appl. Phys. Lett. **92**, 063507 (2008).
[13]C. A. F. Vaz, J. Hoffman, A. B. Posadas, and C. H. Ahn, Appl. Phys. Lett. **94**, 022504 (2009).
[14]G. E. Sterbinsky, B. W. Wessels, J. W. Kim, E. Karapetrova, P. J. Ryan, and D. J. Keavney, Appl. Phys. Lett. **96**, 092510 (2010).
[15]F. Jona and G. Shirane, *Ferroelectric Crystals* (Pergamon, Oxford, 1962), p. 108.
[16]N. M. Nemes, M. Garcia-Hernandez, Z. Szatmari, T. Feher, F. Simon, C. Miller, J. Garcia-Barriocanal, F. Bruno, C. Visani, V. Pena, Z. Sefrioui, C. Leon, and J. Santamaria, IEEE Trans. Magn. **44**, 2926 (2008).
[17]A. J. Millis, T. Darling, and A. Migliori, J. Appl. Phys. **83**, 1588 (1998); A. J. Millis, Nature (London) **392**, 147 (1998).
[18]C. Kwon, M. C. Ronson, K. C. Kim, J. Y. Gu, S. E. Lofland, S. M. Bhagat, Z. Trajanovic, M. Rajeswari, T. Venkatesan, A. R. Kratz, R. D. Gomez, and R. Ramesh, J. Magn. Magn. Mater. **172**, 229 (1997).
[19]T. K. Nath, R. A. Rao, D. Lavric, C. B. Eom, L. Wu, and F. Tsui, Appl. Phys. Lett. **74**, 1615 (1999).
[20]F. Tsui, M. C. Smoak, T. K. Nath, and C. B. Eom, Appl. Phys. Lett. **76**, 2421 (2000).
[21]G. R. Castro, J. Synchrotron Radiat. **5**, 657 (1998).
[22]G. H. Kwei, A. C. Lawson, S. J. L. Billinge, and S. W. Cheong, J. Phys. Chem. **97**, 2368 (1993).
[23]M. Holt, Kh. Hassani, and M. Sutton, Phys. Rev. Lett. **95**, 085504 (2005).
[24]J. M. Colino and A. de Andrés, Appl. Phys. Lett. **87**, 142509 (2005).
[25]A. Hernando and J. M. Barandiaran, J. Phys. D: Appl. Phys. **8**, 833 (1975); Phys. Rev. B **22**, 2445 (1980); A. Hernando, I. Navarro, and J. M. Gonzalez, Europhys. Lett. **20**, 175 (1992).
[26]M. Garcia-Hernandez, J. L. Martinez, M. J. Martinez-Lope, M. T. Casais, and J. A. Alonso, Phys. Rev. Lett. **86**, 2443 (2001).
[27]M. Bibes, S. Valencia, L. Balcells, B. Martinez, J. Fontcuberta, M. Wojcik, S. Nadolski, and E. Jedryka, Phys. Rev. B **66**, 134416 (2003).
[28]$c_{11} = 350$ GPa, $c_{12} = 113$ GPa, and $c_{44} = 150$ GPa: M. Motin Seikh, C. Narayana, L. Sudheendra, A. K. Sood, and C. N. R. Rao, J. Phys. Condens. Matter **16**, 4381 (2004).
[29]$\lambda_{100} = \lambda_{111} = 7 \times 10^{-5}$: J. O'Donnell, M. S. Rzchowski, J. N. Eckstein, and I. Bozovic, Appl. Phys. Lett. **72**, 1775 (1998).
[30]J. M. Barandiaran, A. Hernando, V. Madurga, O. V. Nielsen, M. Vazquez, and M. Vazquez-Lopez, Phys. Rev. B **35**, 5066 (1987).
[31]M. Vazquez, C. Gomez-Polo, D. X. Chen, and A. Hernando, IEEE Trans. Magn. **30**, 907 (1994).
[32]M. Ziese, H. C. Semmelhack, and P. Busch, J. Magn. Magn. Mater. **246**, 327 (2002).
[33]M. Paranjape, A. K. Raychaudhuri, N. D. Mathur, and M. G. Blamire, Phys. Rev. B, **67** 214415 (2003).